

Article

# N-Doped $K_3Ti_5NbO_{14}@TiO_2$ Core-Shell Structure for Enhanced Visible-Light-Driven Photocatalytic Activity in Environmental Remediation

Xin Gao<sup>1,2</sup>, Chen Wang<sup>2</sup>, Qixiang Xu<sup>2</sup>, Hongjie Lv<sup>1</sup>, Ting Chen<sup>1</sup>, Chao Liu<sup>2,\*</sup>  and Xinguo Xi<sup>3,\*</sup>

<sup>1</sup> School of Materials Science and Technology, Jiangsu University, Zhenjiang 212013, China; gaixin\_vv@outlook.com (X.G.); hongjielv\_183@163.com (H.L.); cdszsmct@outlook.com (T.C.)

<sup>2</sup> School of Materials Engineering, Yancheng Institute of Technology, Yancheng 224051, China; dadayc@outlook.com (C.W.); QiaaXiangXu@163.com (Q.X.)

<sup>3</sup> School of Chemistry & Chemical Engineering, Yancheng Institute of Technology, Yancheng 224051, China

\* Correspondence: cliunju@hotmail.com (C.L.); xxg@ycit.cn (X.X.);  
Tel.: +86-515-8829-8251 (C.L.); +86-515-8829-8186 (X.X.)

Received: 29 December 2018; Accepted: 18 January 2019; Published: 21 January 2019



**Abstract:** A novel N-doped  $K_3Ti_5NbO_{14}@TiO_2$  (NTNT) core-shell heterojunction photocatalyst was synthesized by firstly mixing titanium isopropoxide and  $K_3Ti_5NbO_{14}$  nanobelt, and then calcinating at 500 °C in air using urea as the nitrogen source. The samples were analyzed by X-ray diffraction pattern (XRD), scanning electron microscopy (SEM), transmission electron microscopy (TEM), UV-Vis absorption spectroscopy and X-ray photoelectron spectroscopic (XPS) spectra. Anatase  $TiO_2$  nanoparticles were closely deposited on the surface of  $K_3Ti_5NbO_{14}$  nanobelt to form a nanoscale heterojunction structure favorable for the separation of photogenerated charge carriers. Meanwhile, the nitrogen atoms were mainly doped in the crystal lattices of  $TiO_2$ , resulting in the increased light harvesting ability to visible light region. The photocatalytic performance was evaluated by the degradation of methylene blue (MB) under visible light irradiation. The enhanced photocatalytic activity of NTNT was ascribed to the combined effects of morphology engineering, N doping and the formation of heterojunction. A possible photocatalytic mechanism was proposed based on the experimental results.

**Keywords:**  $K_3Ti_5NbO_{14}$  nanobelt;  $TiO_2$ ; core-shell structure; visible-light photodegradation

## 1. Introduction

Nowadays, two main problems of environmental pollution and energy shortage are major challenges with the industrial development, and many organic pollutants will be generated, especially leading to the serious water pollution problem [1,2]. Photocatalysis has been regarded as an efficient approach to solve the above-mentioned problems as they are highly efficient and pollution-free [3–5]. Considering the comprehensive economic benefits, catalytic efficiency, and absence of secondary pollution for this technique, many semiconductor photocatalysts have been widely applied for the removal of produced waste water [6–8]. Among semiconductor photocatalysts,  $TiO_2$  has been widely investigated and commonly used in photocatalytic applications because of its excellent biological and chemical ability, low cost, and nontoxicity [9–12]. However, the pure  $TiO_2$  exhibits the drawbacks of having a wide band gap value and high recombination rate of photogenerated charge carriers, which will cause low quantum efficiency and thus limit its application [13–15]. Therefore, it is necessary to carefully construct photocatalysts with a high efficiency so as to improve photocatalytic activity.

As a typical layered compound,  $K_3Ti_5NbO_{14}$  nanobelts have been well investigated due to their unique layered structure, nanobelt morphology, and electronic properties, in which the anisotropically shaped nanobelts are favorable for the efficient transport of photogenerated electrons and holes, resulting in the decreased recombination rate of photo-induced charge carriers [16]. However, layered  $K_3Ti_5NbO_{14}$  has a relatively large band gap value and thus is difficult to utilize visible light [16]. Thus, it is of great significance to prepare visible-light-response  $K_3Ti_5NbO_{14}$ -based photocatalysts with the increased light harvesting ability and the high photocatalytic efficiency.

Up to now, our group has developed some synergistic methods such as doping, construction of heterojunction, and morphology engineering, to improve the photocatalytic performance of layered titanoniobate [17–20]. For example, a simple calcination method was used to synthesize S-doped mesoporous  $HTiNbO_5/TiO_2$  nanocomposite. The excellent photocatalytic activity for the degradation of rhodamine B (RhB) was attributed to synergistic effects of S doping, the formation of heterojunction, the much larger specific surface area, and richer mesoporosity [19]. Inspired by layered heterojunction, an ordered layered N-doped  $KTiNbO_5/g-C_3N_4$  heterojunction photocatalyst was also constructed, in which such a layered heterojunction was favorable for the efficient separation and transfer of photogenerated charge carriers, resulting in the enhanced visible-light photocatalytic activity for the degradation of RhB and bisphenol A (BPA) [17]. Especially, constructing a hybrid photocatalyst based on  $K_3Ti_5NbO_{14}$  and other semiconductors is an effective approach to improving the photocatalytic activity. The formed heterojunction structure between the two components could achieve an interface and provide a pathway to separate the photogenerated electrons and holes [21]. Therefore, considering the advantages of synergistic effects, it is of great interest to construct a novel  $K_3Ti_5NbO_{14}$ -based photocatalyst using the synergistic effects of doping, the construction of heterojunction, and morphology engineering.

Here, we report a new visible-light-response N-doped  $TiO_2@K_3Ti_5NbO_{14}$  (NTNT) core-shell nanocomposite prepared by a facile one-step calcination route, showing a high photocatalytic activity. The photocatalytic activity was tested by following the degradation of methylene blue (MB) under visible light irradiation. This work discusses the synergistic effect of morphology engineering, N doping and heterojunction on the contribution of photocatalytic activity. A possible mechanism was proposed according to the experimental results.

## 2. Results and Discussion

### 2.1. XRD Analysis

The XRD patterns of the samples are shown in Figure 1. For as-prepared  $K_3Ti_5NbO_{14}$ , all the observed diffraction peaks match well with the published data (JCPDF: No. 72-0908), indicating the high crystallization of  $K_3Ti_5NbO_{14}$  [22]. After coupling with  $TiO_2$ , both  $K_3Ti_5NbO_{14}$  and anatase  $TiO_2$  phases (JCPDF: No. 21-1272) exist in the resulted  $K_3Ti_5NbO_{14}@TiO_2$  (TNT) composite, indicating that the crystal structure of  $K_3Ti_5NbO_{14}$  can be well maintained after the deposition of  $TiO_2$  on its surface. However, the characteristic peaks of  $K_3Ti_5NbO_{14}$  in TNT composite are broaden in comparison with pure  $K_3Ti_5NbO_{14}$ , suggesting the decreased crystallization of TNT derived from the formation of  $TiO_2$  nanoparticles on the surface of  $K_3Ti_5NbO_{14}$  nanobelts. After N doping, with the assistance of urea, the resultant NTNT exhibits similar diffraction peaks to those of TNT. It indicates that the crystal structure of TNT cannot be destroyed during N doping process. Meanwhile, for the sample NTNT, the diffraction peak intensity is slightly decreased and the characteristic peaks are broaden in comparison with TNT. It indicates that the addition of urea for N doping can affect the crystallization.

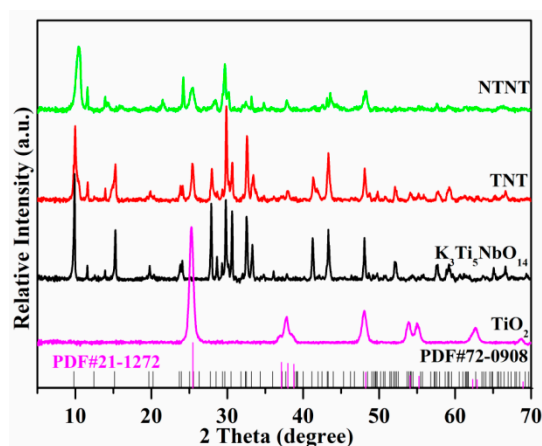


**Figure 1.** XRD patterns of N-doped  $K_3Ti_5NbO_{14}@TiO_2$  (NTNT), TNT,  $K_3Ti_5NbO_{14}$ ,  $TiO_2$ , and the standard patterns of  $K_3Ti_5NbO_{14}$  (JCPDF: No. 72-0908) and  $TiO_2$  (JCPDF: No. 21-1272).

## 2.2. Morphology

Figure 2 shows SEM images of  $K_3Ti_5NbO_{14}$  and NTNT composite. As displayed in Figure 2a, the as-obtained  $K_3Ti_5NbO_{14}$  nanobelts with a smooth surface can be clearly observed with a diameter of a few hundred nanometers and the length of several micrometers. The main reason for the choice of  $K_3Ti_5NbO_{14}$  nanobelts is due to the fact that the long anisotropically shaped nanobelts can provide a pathway for the transport of photogenerated electrons throughout the longitudinal direction, leading to the decreased recombination rate and promoting efficient separation rate of electron–hole pairs [17,23]. After combining  $K_3Ti_5NbO_{14}$  nanobelts with anatase  $TiO_2$  and then N-doping, the surface of the resulting NTNT (Figure 2b) is very rough related to pure  $K_3Ti_5NbO_{14}$ , which may be due to the fact that the  $TiO_2$  nanoparticles were randomly dispersed on the surface of the  $K_3Ti_5NbO_{14}$  to form a  $TiO_2/K_3Ti_5NbO_{14}$  heterojunction structure.

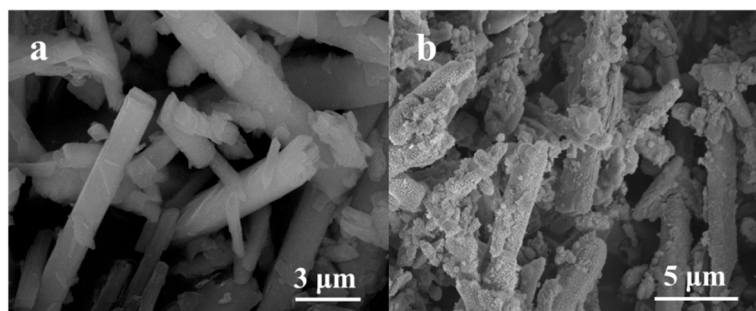


**Figure 2.** FE-SEM images of (a)  $K_3Ti_5NbO_{14}$  and (b) NTNT.

According to TEM image of NTNT (Figure 3a,d), the hierarchical core-shell structure can be clearly visible, and the formed  $TiO_2$  nanoparticles with a size of 18–20 nm are closely deposited on the external surface of  $K_3Ti_5NbO_{14}$  nanobelts, leading to the formation of  $TiO_2/K_3Ti_5NbO_{14}$  heterojunction structure [19]. Additionally, the enlarged HRTEM image of NTNT further confirmed the formation of a hierarchical  $TiO_2@K_3Ti_5NbO_{14}$  core-shell structure. This formed  $TiO_2/K_3Ti_5NbO_{14}$  heterojunction is favorable for promoting the separation efficiency of photogenerated electron–hole pairs at interfaces [24–26]. By enlarging HRTEM images of NTNT (Figure 3b,c), the well-resolved interplanar spacing values are 0.35 nm and 0.28 nm of the external shell and the internal core, respectively. In consideration of the crystallographic symmetry, the external shell is attributed to the anatase  $TiO_2$  nanoparticles with the exposed (101) plane and the internal core is assigned to the presence of  $K_3Ti_5NbO_{14}$  with a (403) plane [22]. The exposed (101) planes in anatase  $TiO_2$  nanoparticles

can act as the possible electron reservoir so as to promote the charge separation based on the previous literature [23,27].

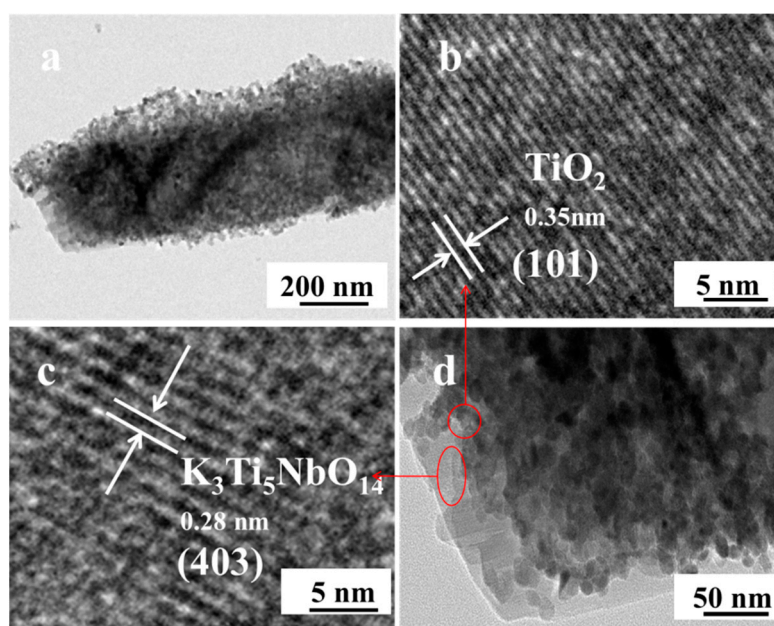


**Figure 3.** (a,d) TEM and HRTEM images of NTNT; (b,c) The enlarged HRTEM images of NTNT.

### 2.3. XPS Studies

The XPS spectra of NTNT were measured to examine the chemical states of the N, Ti and O elements in NTNT. In the total spectrum (Figure 4a), the elements of C, N, Ti and O can be observed, and the existence of the C 1s peak might derive from the examined instrument. As shown in Figure 4b, two peaks at 398.7 and 399.6 eV can be observed in N 1s spectrum. The peak with a low binding energy of 398.7 eV is substituted N in the form of O–Ti–N linkages, in which nitrogen atoms are bonded to Ti atoms and replaced by lattice O atoms in the anatase TiO<sub>2</sub> [28,29]. The peak at 399.6 eV can be attributed to some oxidized states, such as Ti–N–O•••Ti and Ti–O–N•••Ti linkages [30,31]. The binding energy of interstitial N is higher than that of substituted N due to the reduction of the electron density on N resulted from the high electronegativity of O. Considering the unique core-shell structure confirmed by HRTEM image, nitrogen atoms are mainly doped on the anatase TiO<sub>2</sub> shell as the titanoniobate nanoblet core was fully covered with TiO<sub>2</sub> shell and N atoms are difficult doped into the lattice of titanoniobate from the exterior to the interior.

In Figure 4c, there are two peaks at 457.8 eV and 463.8 eV in Ti 2p spectra of NTNT, and these two peaks separately consisted with the orbits splitting of Ti 2p<sub>1/2</sub> and Ti 2p<sub>3/2</sub>, further indicating only the presence of Ti<sup>4+</sup> [32,33]. By comparison, the chemical states of Ti 2p are similar for both K<sub>3</sub>Ti<sub>5</sub>NbO<sub>14</sub> and NTNT. The peak of NTNT (463.8 eV) is higher than that in the K<sub>3</sub>Ti<sub>5</sub>NbO<sub>14</sub> (463.5 eV). These slight shifts are attributed to the presence of a strong interfacial interaction between TiO<sub>2</sub> and K<sub>3</sub>Ti<sub>5</sub>NbO<sub>14</sub> [24,34]. As displayed in Figure 4d, for the sample of pure K<sub>3</sub>Ti<sub>5</sub>NbO<sub>14</sub>, two fitting peaks of 529.3 and 530.8 eV are ascribed to lattice oxygen in composite and oxynitride (or adsorbed water), respectively. Moreover, a slight shift is also observed for O 1s spectra, further indicating the presence of a strong interfacial interaction between TiO<sub>2</sub> and K<sub>3</sub>Ti<sub>5</sub>NbO<sub>14</sub>.

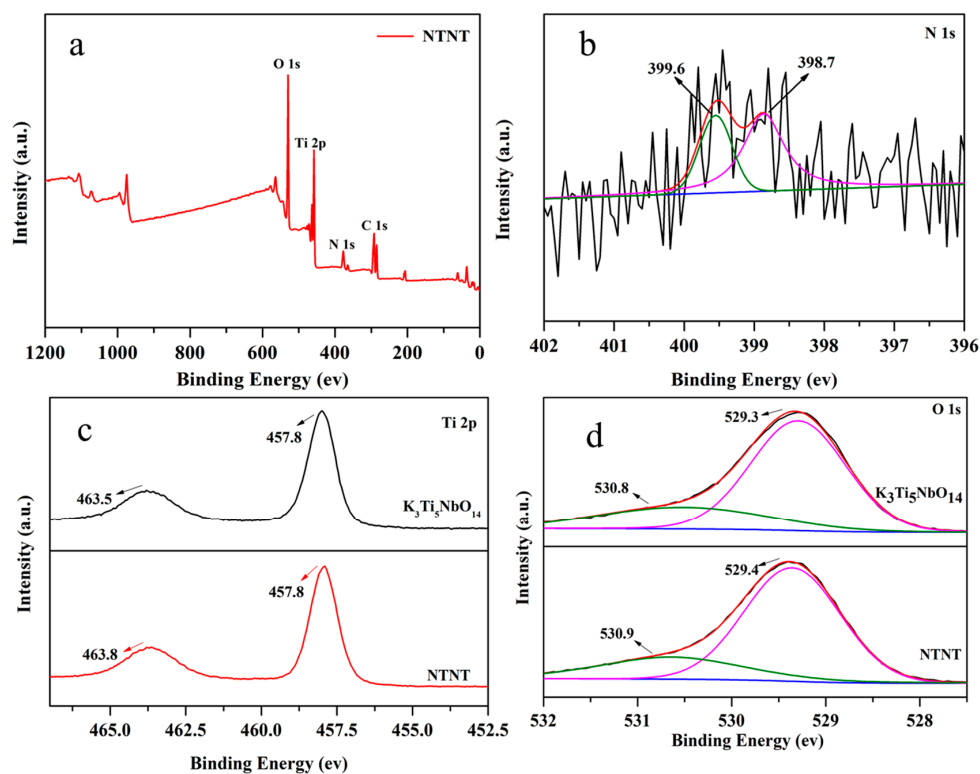


**Figure 4.** XPS spectra of NTNT: (a) Total spectra. (b) N1s spectra. (c) Ti 2p spectra. (d) O 1s spectra.

#### 2.4. UV-Vis Diffuse Reflectance Spectra

The UV-Vis diffuse reflectance spectra of as-prepared samples were shown in Figure 5. For pure  $K_3Ti_5NbO_{14}$ , only an absorption band can be observed in the UV region due to the band-to-band transition [19], and the band gap value is  $\sim 3.95$  eV based on our previous work [22]. After hybridization with  $TiO_2$ , the resultant TNT exhibits an enhanced absorption in UV-light region, which is mainly due to the formation of  $K_3Ti_5NbO_{14}/TiO_2$  heterojunction and possible quantum size effect [35]. The absorbance edge of TNT is shifted to about 390 nm. Based on previous literature [15], the band gaps of NTNT, TNT,  $TiO_2$ , and N- $TiO_2$  were calculated to be 2.81, 3.18, 3.20, and 2.90 eV from the onset of the absorption edge, respectively.

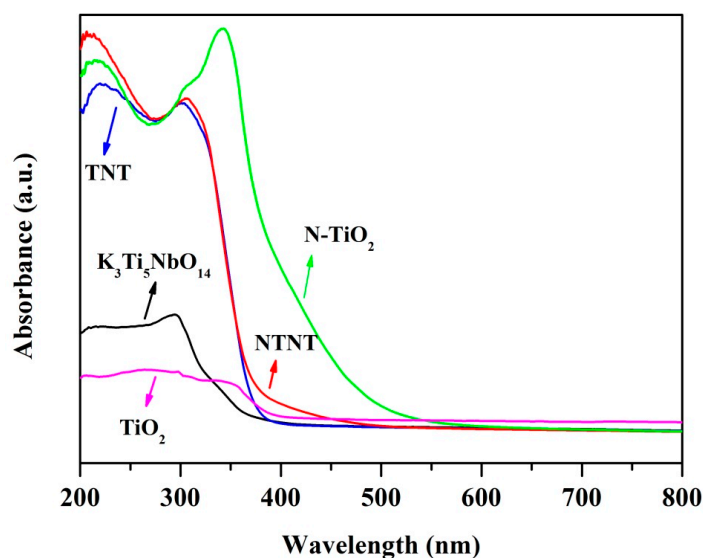


**Figure 5.** UV-Vis diffuse reflectance spectra (DRS) of  $K_3Ti_5NbO_{14}$ , TNT, NTNT,  $TiO_2$ , and N- $TiO_2$ .

After N doping, the absorption in both UV and visible light region can be clearly visible for the resulted NTNT, and the absorbance edge is further profoundly shifted to 475 nm related to the sample of TNT, which also indicates that N TNT has a potential great visible light harvesting ability. The N-TiO<sub>2</sub> is as a standard sample also confirmed the N-doping could enlarge the light response.

### 2.5. Photocatalytic Performance

As displayed in Figure 6, the characterized photocatalytic efficiency of samples was evaluated by degrading MB under visible light irradiation [36,37]. The self-degradation of pure MB solution without any catalyst can be ignored. For pure K<sub>3</sub>Ti<sub>5</sub>NbO<sub>14</sub> and TiO<sub>2</sub>, only 30% and 20% of MB solution could be respectively degraded under visible light irradiation within 50 min due to the self-photosensitization. After hybridizing K<sub>3</sub>Ti<sub>5</sub>NbO<sub>14</sub> with TiO<sub>2</sub>, the resultant TNT shows an enhanced photocatalytic activity for the degradation of MB compared to pure K<sub>3</sub>Ti<sub>5</sub>NbO<sub>14</sub>, which is mainly attributed to the formation of heterojunction structure between K<sub>3</sub>Ti<sub>5</sub>NbO<sub>14</sub> and TiO<sub>2</sub>. Additionally, the N-TiO<sub>2</sub> shows a relatively low photocatalytic activity, confirming that the just broaden light response region not the only reason for the high photocatalytic activity. After further doping with nitrogen atoms, the sample of NTNT shows a higher photocatalytic activity than that of TNT, indicating that N doping can improve the light harvesting ability. Thus, the synergistic effects of morphology engineering, N doping and the formation of heterojunction could greatly improve the photocatalytic activity efficiently.

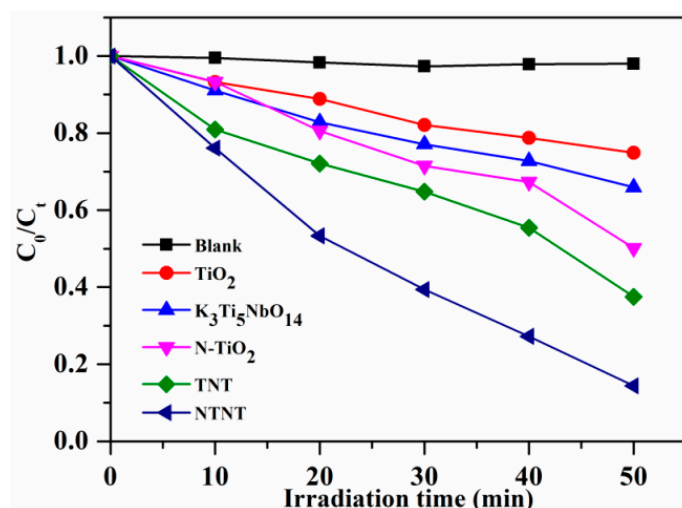


**Figure 6.** Visible light photocatalytic degradation rate of methylene blue (MB) solution for different samples.

Five time reused experiment in Figure 7 were taken to examine the stability of catalyst in the photocatalytic process. There is no obvious deactivation of the photocatalyst after reused experiment for five times. It indicates the NTNT still has a great photocatalytic activity and stability for the degradation of MB under visible light irradiation.

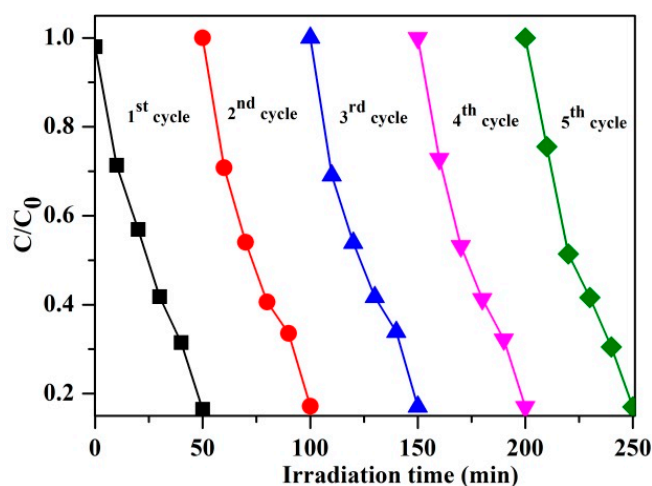


**Figure 7.** Cycling experiments of NTNT for MB degradation under visible light irradiation.

### 2.6. Photocatalytic Mechanism Discussion

In order to study the separation and migration rate of photoinduced electrons and holes, the transient photocurrent responses (Figure 8) were measured for the samples of  $K_3Ti_5NbO_{14}$ , TNT and NTNT. A constant photocurrent can be formed when the photogenerated electrons and holes reaches the equilibrium, while the decay of the photocurrent means the quick recombination of electrons and holes [38,39]. It is obvious that the  $K_3Ti_5NbO_{14}$  shows the weakest visible light response due to the original wide band gap of pure  $K_3Ti_5NbO_{14}$ . After combining with  $TiO_2$ , the photocurrent intensity of TNT is nearly 2 times than that of the  $K_3Ti_5NbO_{14}$ , which may be due to the promoted separation of photogenerated charge carriers and accelerated transfer of the interfacial charge derived from the formed heterojunction structure [40,41]. After further doping by N, the sample of NTNT shows the higher photocurrent intensity than TNT. It indicates that both the formation of heterojunction and N doping can effectively promote the separation of photogenerated charge carriers.

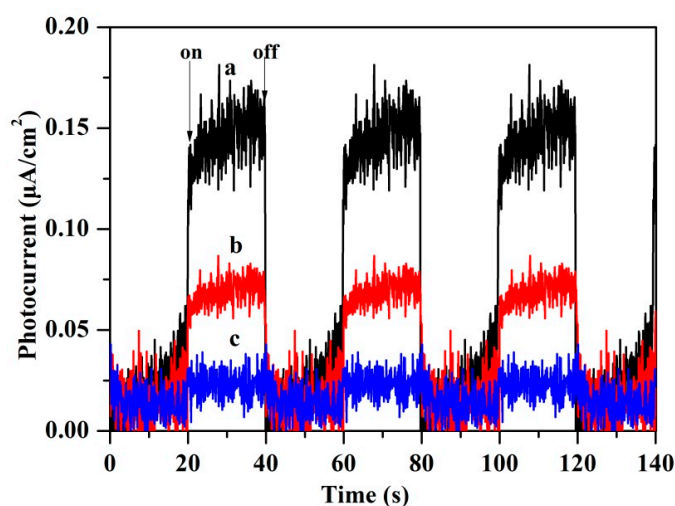


**Figure 8.** Photocurrent responses of (a) NTNT, (b) TNT, and (c)  $K_3Ti_5NbO_{14}$ .

The photoluminescence (PL) technique has been widely employed to investigate the migration, transfer, and recombination process of photoinduced electrons and holes in semiconductors [42,43]. The high emission intensity indicates the fast recombination rate of electron–hole pairs. As displayed in Figure 9, the broad peak at 643 nm of  $K_3Ti_5NbO_{14}$  with the excitation wavelength of 320 nm is attributed to the band gap recombination of electron–hole pairs. After hybridizing with  $TiO_2$ ,

a drastically decreased PL intensity can be observed in TNT, indicating the formation of heterojunction can effectively accelerate the separation of photogenerated electrons and holes. After N doping, the PL intensity of NTNT is further decreased, indicating the synergistic effects of heterojunction and N doping can profoundly accelerate the separation of photogenerated electrons and holes.

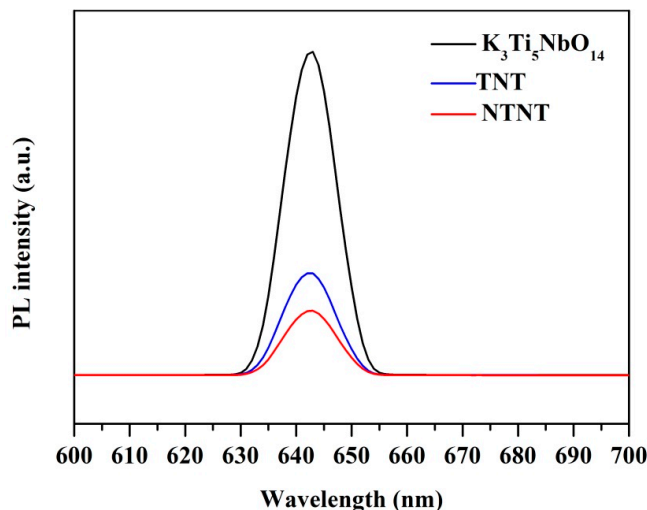


Figure 9. PL spectra of NTNT, TNT, and  $K_3Ti_5NbO_{14}$ .

Based on the above results, a possible photocatalytic mechanism for the degradation of MB is proposed and schematically displayed in Figure 10. Under visible light irradiation, only NTNT can be generated to produce electrons and holes, while pure  $K_3Ti_5NbO_{14}$  cannot due to the large band gap. The photogenerated electrons are transferred from N 2p state to CB of anatase  $TiO_2$ , while the formed holes are also left in the N 2p state. As the energy potentials are different between  $K_3Ti_5NbO_{14}$  and  $TiO_2$ , the photogenerated electrons are further transferred from CB of anatase  $TiO_2$  to CB of  $K_3Ti_5NbO_{14}$ , leading to the efficient separation and transfer of photoinduced charge carriers. Furthermore, the long anisotropically shaped nanobelts can provide a pathway for the transport of photogenerated electrons throughout the longitudinal direction. The exposed (101) facets can act as in anatase  $TiO_2$  nanoparticles can act as the possible electron reservoir so as to promote the charge separation.

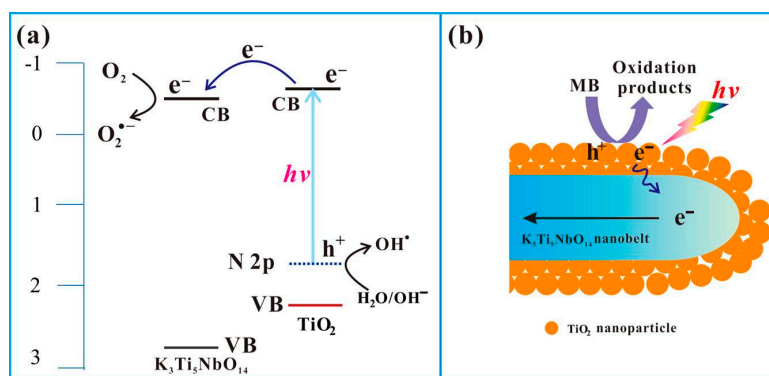


Figure 10. A possible photocatalytic mechanism of the NTNT for the photodegradation of the organic pollutants.

The photogenerated electrons in CB of  $K_3Ti_5NbO_{14}$  can react with dissolved  $O_2$  to generate  $O_2^{\bullet-}$ , and the formed holes in VB of anatase  $TiO_2$  can react with  $OH^-$  groups or  $H_2O$  molecules to produce  $\bullet OH$  radicals. The produced  $O_2^{\bullet-}$  and  $\bullet OH$  are able to oxidize organic pollutant of MB owing to their high oxidization ability.

### 3. Materials and Methods

#### 3.1. Preparation of N-doped $K_3Ti_5NbO_{14}@TiO_2$ Nanocomposite

All the raw materials were used in this experimental without any further purification. Layered  $K_3Ti_5NbO_{14}$  was prepared by first fully grinding and then calcinating a mixture of  $K_2CO_3$ ,  $TiO_2$  and  $Nb_2O_5$  (molar ratios: 3:10:1) at 1050 °C for 24 h with a heating rate of 5 °C/min.

2.0 g of as-prepared  $K_3Ti_5NbO_{14}$  was well dispersed in 50 mL ethanol with an ultrasonic treatment for 30 min and then magnetic stirring for 4 h in the sealed beaker. After the well distribution of the obtained suspension, 2 mL of titanium isopropoxide was added into the above suspension dropwise and kept stirring in the air. After the total evaporation of the ethanol, 1.0 g of the obtained precursor was milled with 2.0 g of urea and then heated at 500 °C for 5 h with a heating rate of 2 °C/min. The resulted yellow sample was washed with distilled water for several times. The resulted N-doped  $K_3Ti_5NbO_{14}@TiO_2$  composite was denoted as NTNT. For comparison, undoped sample of  $K_3Ti_5NbO_{14}@TiO_2$  (denoted as TNT) composite was also prepared according to the similar processes of N-doped  $K_3Ti_5NbO_{14}@TiO_2$  without the addition of urea. N-doped  $TiO_2$  (denoted as N- $TiO_2$ ) was also prepared similar to the above experimental processes without layered  $K_3Ti_5NbO_{14}$ . Anatase  $TiO_2$  was prepared similar to the above experimental processes without layered  $K_3Ti_5NbO_{14}$  and the addition of urea.

#### 3.2. Characterization

Powder X-ray diffraction (XRD) patterns of the obtained samples were taken on a Philip-X'Pert X-ray diffractometer (Philip, Amsterdam, Netherlands) with a Cu K $\alpha$  radiation ( $\lambda = 1.5418 \text{ \AA}$ ), at a scanning rate of 0.2 °/s in a range of 5~70°. Ultraviolet visible diffuse reflectance spectra were obtained on a UV-Vis spectrophotometer (Shimadzu, UV-3600 plus, Kyoto, Japan) in a range of 200–800 nm. The morphology was investigated by field-emission scanning electron microscopy (FE-SEM, Nano SEM 450) and transmission electron microscopy (HRTEM, JEOL JEM-2100F, Tokyo, Japan) with an accelerate voltage of 200 kV. For HRTEM observation, the sample was well dispersed in ethanol with an ultrasonic treatment and then dropped onto carbon-coated copper grids. The X-ray photoelectron spectroscopic (XPS) analysis was carried out on an X-ray photoelectron spectrometer (Thermo Fisher Scientific, K-Alpha, Waltham, MA, USA) equipped with a hemispherical electron analyzer (pass energy of 20 eV) and an Al K ( $h\nu = 1361 \text{ eV}$ ) X-ray source. The binding energies (BE) were referenced to the adventitious C 1s peak (284.8 eV) as an internal standard to consider charging effects. Photoluminescence (PL) spectra were obtained on a F4500 (Hitachi, Tokyo, Japan) luminescence spectrometer at room temperature.

The time-photocurrent curve tested by a three-electrode system on CHI660D, Pt slice as a counter electrode, calomel electrode as a reference electrode and the ITO work electrode with a Xe lamp (300 W) as a light resource. The tests were taken in a PBS (0.1M disodium hydrogen phosphate and sodium dihydrogen phosphate mixing aqueous solution, pH = 7) and turn on/off the light on an interval of 20 s. The preparation method of the working electrode is as follows: 2 cm  $\times$  2 cm ITO conductive glass is cleaned by a certain proportion of hydrogen peroxide (1 mL, 30%), ammonium hydroxide (1 mL, 28%) and distilled water (50 mL) with a supersonic cleaning for 15 minutes, and then ITO is dried in an air-blast drying box at 80 °C. The ITO conductive surface is sealed by Scotch tape to expose the square with an area of 1 cm  $\times$  1 cm. After a 30 mg sample was added to 1 ml water solution for 30 minutes, the suspension droplets were diluted and dried naturally on ITO surface. A working electrode can be obtained tear the Scotch tape off and dry the ITO at 80 °C.

#### 3.3. Photocatalytic Test

The photocatalytic activity was measured by degrading the methylene blue (MB,  $2 \times 10^{-2} \text{ g/L}$ ) aqueous solution under visible light irradiation. Fifty milligrams of the catalyst was firstly added into 100 mL of MB solution and stirred continuously for 1 h in darkness in order to acquire an adsorption–desorption equilibrium. The Xe-lamp (300 W) with a filter to make  $\lambda > 420 \text{ nm}$  was used

as a visible light source. The overall photocatalytic test was carried under a circular water system to remove the heating effect. At appropriate time intervals after irradiation, about 4 mL of suspension was centrifuged and then measured by UV-Vis spectrum (ultraviolet-visible spectroscopy) to calculate the degrading efficiency  $C_t/C_0$ , where  $C_t$  and  $C_0$  were the concentration at the time  $t$  and the initial concentration respectively. To further study the photostability of the catalyst, we also took a cycling experiment for five times with the same photocatalytic test processes above mentioned. After each cycling, the catalyst was accumulated by a filter with a micro-pore diameter of 0.45  $\mu\text{m}$ . Then, the acquired catalyst was washed with distilled water for further use.

#### 4. Conclusions

In this work, a facile one-step calcination method was developed to synthesize a novel N-doped  $\text{K}_3\text{Ti}_5\text{NbO}_{14}@\text{TiO}_2$  core-shell heterojunction photocatalyst, in which  $\text{K}_3\text{Ti}_5\text{NbO}_{14}$  nanobelts were firstly mixed with titanium isopropoxid, and then calcinated at 500 °C in air using urea as the nitrogen source for N doping treatment. The formed anatase  $\text{TiO}_2$  nanoparticles were closely deposited on the surface of  $\text{K}_3\text{Ti}_5\text{NbO}_{14}$  nanobelt to form a heterojunction structure between two components, which was favorable for the transfer and separation of photogenerated charge carriers. In consideration of the unique core-shell structure, nitrogen atoms were mainly incorporated into the crystal lattices of  $\text{TiO}_2$  shell, resulting in the increased light harvesting ability to visible light region. The photocatalytic performance was evaluated by the degradation of methylene blue (MB) under visible light irradiation. The resulted sample of NTNT showed the enhanced photocatalytic activity owing to the synergistic effects of morphology engineering, N doping and the formation of heterojunction. A possible photocatalytic mechanism was proposed based on the experimental results.

**Author Contributions:** The experimental work was designed and supported by L.C. and X.X. C.W. and Q.X. helped performed the precursors; X.G., H.L. and T.C. analyzed the data; C.L. and X.X. contributed reagents/materials/analysis tools and all materials supports; The manuscript was amended and supplemented by all authors. All authors have given approval for the final version of the manuscript.

**Funding:** The authors greatly appreciate the financial support of, National Natural Science Foundation of China (No. 51772258), Natural Science Foundation of Jiangsu Province (No. BK20160434), National Key Research and Development Project (No. 2016YFC0209202), China Postdoctoral Science Foundation (No. 2018M632283), National Key Research and Development Project (No. 2016YFC0209202), Industry–University–Research Collaboration Project of Jiangsu Province (No. BY2018281), Natural Science Foundation of the Jiangsu Higher Education Institutions of China (No. 15KJA430007), Special Foundation for Novel Wall Materials of Jiangsu Province (No. 201614), Yancheng Agricultural Science and Technology Innovation Special Guiding Foundation Project (No. YK2016031).

**Conflicts of Interest:** The authors declare no conflict of interest.

#### References

1. Stolarczyk, J.K.; Bhattacharyya, S.; Polavarapu, L.; Feldmann, J. Challenges and prospects in solar water splitting and  $\text{CO}_2$  reduction with inorganic and hybrid nanostructures. *ACS Catal.* **2018**, *8*, 3602–3635. [[CrossRef](#)]
2. Chu, S.; Cui, Y.; Liu, N. The path towards sustainable energy. *Nat. Mater.* **2016**, *16*, 16. [[CrossRef](#)] [[PubMed](#)]
3. Zhou, C.; Lai, C.; Zhang, C.; Zeng, G.; Huang, D.; Cheng, M.; Hu, L.; Xiong, W.; Chen, M.; Wang, J.; et al. Semiconductor/boron nitride composites: Synthesis, properties, and photocatalysis applications. *Appl. Catal. B Environ.* **2018**, *238*, 6–18. [[CrossRef](#)]
4. Ganguly, P.; Byrne, C.; Breen, A.; Pillai, S.C. Antimicrobial activity of photocatalysts: Fundamentals, mechanisms, kinetics and recent advances. *Appl. Catal. B Environ.* **2018**, *225*, 51–75. [[CrossRef](#)]
5. Fu, J.; Yu, J.; Jiang, C.; Cheng, B. g- $\text{C}_3\text{N}_4$ -Based heterostructured photocatalysts. *Adv. Energy Mater.* **2018**, *8*, 1701503. [[CrossRef](#)]
6. He, R.; Xu, D.; Cheng, B.; Yu, J.; Ho, W. Review on nanoscale Bi-based photocatalysts. *Nanoscale Horiz.* **2018**, *3*, 464–504. [[CrossRef](#)]
7. Marschall, R. Semiconductor Composites: Strategies for enhancing charge carrier separation to improve photocatalytic activity. *Adv. Funct. Mater.* **2014**, *24*, 2421–2440. [[CrossRef](#)]

8. Schneider, J.; Matsuoka, M.; Takeuchi, M.; Zhang, J.; Horiuchi, Y.; Anpo, M.; Bahnemann, D.W. Understanding TiO<sub>2</sub> photocatalysis: Mechanisms and materials. *Chem. Rev.* **2014**, *114*, 9919–9986. [[CrossRef](#)]
9. Zhai, Z.; Hu, C.H.; Yang, X.Y.; Zhang, L.H.; Liu, C.; Fan, Y.N.; Hou, W.H. Nitrogen-doped mesoporous nanohybrids of TiO<sub>2</sub> nanoparticles and HTiNbO<sub>5</sub> nanosheets with a high visible-light photocatalytic activity and a good biocompatibility. *J. Mater. Chem.* **2012**, *22*, 19122–19131. [[CrossRef](#)]
10. Liu, C.; Liang, J.Y.; Han, R.R.; Wang, Y.Z.; Zhao, J.; Huang, Q.J.; Chen, J.; Hou, W.H. S-doped Na<sub>2</sub>Ti<sub>6</sub>O<sub>13</sub>@TiO<sub>2</sub> core-shell nanorods with enhanced visible light photocatalytic performance. *Phys. Chem. Chem. Phys.* **2015**, *17*, 15165–15172. [[CrossRef](#)]
11. Sang, L.; Zhao, Y.; Burda, C. TiO<sub>2</sub> nanoparticles as functional building blocks. *Chem. Rev.* **2014**, *114*, 9283–9318. [[CrossRef](#)] [[PubMed](#)]
12. Zhang, A.Y.; Wang, W.; Chen, J.J.; Liu, C.; Li, Q.; Zhang, X.; Li, W.W.; Si, Y.; Yu, H.Q. Epitaxial facet junction on TiO<sub>2</sub> single crystals for efficient photocatalytic water splitting. *Energy Environ. Sci.* **2018**, *11*, 6. [[CrossRef](#)]
13. Chen, X.; Liu, L.; Huang, F. Black titanium dioxide (TiO<sub>2</sub>) nanomaterials. *Chem. Soc. Rev.* **2015**, *44*, 1861–1885. [[CrossRef](#)] [[PubMed](#)]
14. Lu, Z.; Zeng, L.; Song, W.; Qin, Z.; Zeng, D.; Xie, C. In situ synthesis of C-TiO<sub>2</sub>/g-C<sub>3</sub>N<sub>4</sub> heterojunction nanocomposite as highly visible light active photocatalyst originated from effective interfacial charge transfer. *Appl. Catal. B Environ.* **2017**, *202*, 489–499. [[CrossRef](#)]
15. D’Amato, C.A.; Giovannetti, R.; Zannotti, M.; Rommozzi, E.; Ferraro, S.; Seghetti, C.; Minicucci, M.; Gunnella, R.; Cicco, A.D. Enhancement of visible-light photoactivity by polypropylene coated plasmonic Au/TiO<sub>2</sub> for dye degradation in water solution. *Appl. Surf. Sci.* **2018**, *441*, 575–587. [[CrossRef](#)]
16. Park, S.; Lee, J.M.; Jo, Y.K.; Kim, I.Y.; Hwang, S.J. A facile exfoliation-crystal growth route to multicomponent Ag<sub>2</sub>CO<sub>3</sub>/Ag-Ti<sub>5</sub>NbO<sub>14</sub> nanohybrids with improved visible light photocatalytic activity. *Dalton. Trans.* **2014**, *43*, 10566–10573. [[CrossRef](#)] [[PubMed](#)]
17. Liu, C.; Zhu, H.; Dong, P.Y.; Hou, H.; Xu, Q.; Chen, X.; Xi, X.; Hou, W. Ordered layered N-doped KTiNbO<sub>5</sub>/g-C<sub>3</sub>N<sub>4</sub> heterojunction with enhanced visible light photocatalytic activity. *Appl. Catal. B Environ.* **2018**, *228*, 54–63. [[CrossRef](#)]
18. Liu, C.; Zhang, C.; Wang, J.; Xu, Q.; Chen, X.; Wang, C.; Xi, X.; Hou, W. N-doped CsTi<sub>2</sub>NbO<sub>7</sub>@g-C<sub>3</sub>N<sub>4</sub> core-shell nanobelts with enhanced visible light photocatalytic activity. *Mater. Lett.* **2018**, *217*, 235–238. [[CrossRef](#)]
19. Liu, C.; Han, R.; Ji, H.; Sun, T.; Zhao, J.; Chen, N.; Chen, J.; Guo, X.; Hou, W.; Ding, W. S-doped mesoporous nanocomposite of HTiNbO<sub>5</sub> nanosheets and TiO<sub>2</sub> nanoparticles with enhanced visible light photocatalytic activity. *Phys. Chem. Chem. Phys.* **2016**, *18*, 801–810. [[CrossRef](#)]
20. Liu, C.; Wu, L.; Chen, J.; Liang, J.Y.; Li, C.S.; Ji, H.M.; Hou, W.H. The nanocomposite of polyaniline and nitrogen-doped layered HTiNbO<sub>5</sub> with excellent visible-light photocatalytic performance. *Phys. Chem. Chem. Phys.* **2014**, *16*, 13409–13417. [[CrossRef](#)]
21. Liu, C.; Wu, Q.; Ji, M.; Zhu, H.; Hou, H.; Yang, Q.; Jiang, C.; Wang, J.; Tian, L.; Chen, J.; et al. Constructing Z-scheme charge separation in 2D layered porous BiOBr/graphitic C<sub>3</sub>N<sub>4</sub> nanosheets nanojunction with enhanced photocatalytic activity. *J. Alloy Compd.* **2017**, *723*, 1121–1131. [[CrossRef](#)]
22. Liu, C.; Xu, G.; Zhu, Y.; Xu, Q.; Yu, G.; Hou, H.; Xu, Q.; Xi, X.; Hou, W. In situ construction of layered K<sub>3</sub>Ti<sub>5</sub>NbO<sub>14</sub>/g-C<sub>3</sub>N<sub>4</sub> composite for improving visible-light-driven photocatalytic performance. *J. Mater. Sci. Mater. Electron.* **2018**, *29*, 15859–15868. [[CrossRef](#)]
23. D’Arienzo, M.; Carbajo, J.; Bahamonde, A.; Crippa, M.; Polizzi, S.; Scotti, R.; Wahba, L.; Morazzoni, F. Photogenerated defects in shape-controlled TiO<sub>2</sub> anatase nanocrystals: A probe to evaluate the role of crystal facets in photocatalytic processes. *J. Am. Chem. Soc.* **2011**, *133*, 17652–17661. [[CrossRef](#)] [[PubMed](#)]
24. Fu, J.; Xu, Q.; Low, J.; Jiang, C.; Yu, J. Ultrathin 2D/2D WO<sub>3</sub>/g-C<sub>3</sub>N<sub>4</sub> step-scheme H<sub>2</sub>-production photocatalyst. *Appl. Catal. B Environ.* **2019**, *243*, 556–565. [[CrossRef](#)]
25. Zhao, H.; Hu, Z.; Liu, J.; Li, Y.; Wu, M.; Tendeloo, G.V.; Su, B.-L. Blue-edge slow photons promoting visible-light hydrogen production on gradient ternary 3DOM TiO<sub>2</sub>-Au-CdS photonic crystals. *Nano Energy* **2018**, *47*, 266–274. [[CrossRef](#)]
26. Xu, F.; Zhang, J.; Zhu, B.; Yu, J.; Xu, J. CuInS<sub>2</sub> sensitized TiO<sub>2</sub> hybrid nanofibers for improved photocatalytic CO<sub>2</sub> reduction. *Appl. Catal. B Environ.* **2018**, *230*, 194–202. [[CrossRef](#)]
27. Liu, G.; Yang, H.G.; Pan, J.; Yang, Y.Q.; Lu, G.Q.; Cheng, H.M. Titanium dioxide crystals with tailored facets. *Chem. Rev.* **2014**, *114*, 9559–9612. [[CrossRef](#)] [[PubMed](#)]

28. Lee, H.U.; Lee, S.C.; Choi, S.; Son, B.; Kim, H.; Lee, S.M.; Kim, H.J.; Lee, J. Influence of visible-light irradiation on physicochemical and photocatalytic properties of nitrogen-doped three-dimensional (3D) titanium dioxide. *J. Hazard. Mater.* **2013**, *258*–259, 10–18. [[CrossRef](#)]
29. Ou, H.H.; Lo, S.L.; Liao, C.H. N-Doped TiO<sub>2</sub> Prepared from microwave-assisted titanate nanotubes (Na<sub>x</sub>H<sub>2-x</sub>Ti<sub>3</sub>O<sub>7</sub>): The effect of microwave irradiation during TNT synthesis on the visible light photoactivity of N-doped TiO<sub>2</sub>. *J. Phys. Chem. C* **2011**, *115*, 4000–4007. [[CrossRef](#)]
30. Li, H.; Li, J.; Huo, Y. Highly active TiO<sub>2</sub>N photocatalysts prepared by treating TiO<sub>2</sub> precursors in NH<sub>3</sub>/ethanol fluid under supercritical conditions. *J. Phys. Chem. B* **2006**, *110*, 1559–1565. [[CrossRef](#)]
31. Yang, X.; Cao, C.; Erickson, L.; Hohn, K.; Maghirang, R.; Klabunde, K. Photocatalytic degradation of Rhodamine B on C-, S-, N-, and Fe-doped TiO<sub>2</sub> under visible-light irradiation. *Appl. Catal. B Environ.* **2009**, *91*, 657–662. [[CrossRef](#)]
32. Pulsipher, D.J.V.; Martin, I.T.; Fisher, E.R. Controlled nitrogen doping and film colorimetrics in porous TiO<sub>2</sub> materials using plasma processing. *ACS Appl. Mater. Interfaces* **2010**, *2*, 1743–1753. [[CrossRef](#)] [[PubMed](#)]
33. Schafranek, R.; Payan, S.; Maglione, M.; Klein, A. Barrier height at (Ba, Sr)TiO<sub>3</sub>/Pt interfaces studied by photoemission. *Phys. Rev.* **2008**, *77*, 195310. [[CrossRef](#)]
34. Jiang, D.; Wen, B.; Zhang, Y.; Jin, Y.; Li, D.; Chen, M. MoS<sub>2</sub>/SnNb<sub>2</sub>O<sub>6</sub> 2D/2D nanosheet heterojunctions with enhanced interfacial charge separation for boosting photocatalytic hydrogen evolution. *J. Colloid Interface Sci.* **2019**, *536*, 1–8. [[CrossRef](#)] [[PubMed](#)]
35. Chen, Z.J.; Lin, B.Z.; Chen, Y.L.; Zhang, K.Z.; Li, B.; Zhu, H. Pillaring and photocatalytic properties of mesoporous α-Fe<sub>2</sub>O<sub>3</sub>/titanate nanocomposites via an exfoliation and restacking route. *J. Phys. Chem. Solids* **2010**, *71*, 841–847. [[CrossRef](#)]
36. Tian, L.; Sun, K.; Rui, Y.; Cui, W.; An, W. Facile synthesis of an Ag@AgBr nanoparticle-decorated K<sub>4</sub>Nb<sub>6</sub>O<sub>17</sub> photocatalyst with improved photocatalytic properties. *RSC Adv.* **2018**, *8*, 29309–29320. [[CrossRef](#)]
37. Zhang, J.; Zhang, L.L.; Shi, Y.X.; Xu, G.L.; Zhang, E.P.; Wang, H.B.; Kong, Z.; Xi, J.H.; Ji, Z.G. Anatase TiO<sub>2</sub> nanosheets with coexposed {101} and {001} facets coupled with ultrathin SnS<sub>2</sub> nanosheets as a face-to-face n-p-n dual heterojunction photocatalyst for enhancing photocatalytic activity. *Appl. Surf. Sci.* **2017**, *420*, 839–848. [[CrossRef](#)]
38. Wang, K.; Li, Y.; Zhang, G.; Li, J.; Wu, X. 0D Bi nanodots/2D Bi<sub>3</sub>NbO<sub>7</sub> nanosheets heterojunctions for efficient visible light photocatalytic degradation of antibiotics: Enhanced molecular oxygen activation and mechanism insight. *Appl. Catal. B Environ.* **2019**, *240*, 39–49. [[CrossRef](#)]
39. Zhu, Y.; Marianov, A.; Xu, H.; Lang, C.; Jiang, Y. Bimetallic Ag–Cu supported on graphitic carbon nitride nanotubes for improved visible-light photocatalytic hydrogen production. *ACS Appl. Mater. Interfaces* **2018**, *10*, 9468–9477. [[CrossRef](#)]
40. Zhao, X.; Huang, S.; Liu, Y.; Liu, Q.; Zhang, Y. In situ preparation of highly stable polyaniline/W<sub>18</sub>O<sub>49</sub> hybrid nanocomposite as efficient visible light photocatalyst for aqueous Cr(VI) reduction. *J. Hazard. Mater.* **2018**, *353*, 466–475. [[CrossRef](#)]
41. Ye, F.; Li, H.; Yu, H.; Chen, S.; Quan, X. Constructing BiVO<sub>4</sub>-Au@CdS photocatalyst with energetic charge-carrier-separation capacity derived from facet induction and Z-scheme bridge for degradation of organic pollutants. *Appl. Catal. B Environ.* **2018**, *227*, 258–265. [[CrossRef](#)]
42. Rommozzi, E.; Zannotti, M.; Giovannetti, R.; D’Amato, C.A.; Ferraro, S.; Minicucci, M.; Gunnella, R.; Cicco, A.D. Reduced graphene oxide/TiO<sub>2</sub> nanocomposite: From synthesis to characterization for efficient visible light photocatalytic applications. *Catalysts* **2018**, *8*, 598. [[CrossRef](#)]
43. D’Amato, C.A.; Giovannetti, R.; Zannotti, M.; Rommozzi, E.; Minicucci, M.; Gunnella, R.; Cicco, A.D. Band gap implications on nano-TiO<sub>2</sub> surface modification with ascorbic acid for visible light-active polypropylene coated photocatalyst. *Nanomaterials* **2018**, *8*, 599. [[CrossRef](#)] [[PubMed](#)]

